American Mineralogist, Volume 75, pages 267–275, 1990

Layer-stacking sequences and structural disorder in mixed-layer illite/smectite: Image simulations and HRTEM imaging

Jung Ho Ahn
Department of Geology, Arizona State University, Tempe, Arizona 85287-1404, U.S.A.
Peter R. Buseck
Departments of Geology and Chemistry, Arizona State University, Tempe, Arizona 85287-1404, U.S.A.

Abstract

R1- and R3-ordered mixed-layer illite/smectite (I/S) samples with 10, 18, and 30% expandable layers were investigated by high-resolution transmission electron microscopy (HRTEM) at 400 kV. In both R1 and R3 I/S samples, $1M_d$ stacking dominates; in many crystals, stacking faults limit *1M* order to only two or three layers. Although a high degree of stacking disorder largely accounts for $1M_d$ characteristics as seen in X-ray diffraction patterns, HRTEM images indicate that individual 2:1 layers of I/S have slightly different β values. Such structural heterogeneity of individual layers also contributes to the weakness or absence of *hkl* reflections. In one R3 I/S crystal (with 10% expandable layers), localized $2M_1$-like stacking occurs within a disordered stacking sequence.

Simulated images show significant differences between illite and smectite interlayers, but they cannot be differentiated in experimental images. Although the concept of fundamental particles (Nadeau et al., 1984a, 1984b, 1984c) implies that 20- and 40-Å-thick particles dominate in R1 and R3 I/S, respectively, consistent packet thicknesses showing the characteristics of fundamental particles are not observed in our specimens. All structure images show regions with coherent stacking, most of which are at least two or three times thicker than the predicted fundamental particles of Nadeau and coworkers. This observation supports the suggestion of Ahn and Peacor (1986b) that thin "fundamental particles" are secondary crystallites derived from larger crystals by cleaving at smectite interlayers during sample preparation.

Introduction

Mixed-layer illite/smectite (I/S) is widespread in sedimentary and low-grade metamorphic rocks. Its chemical and structural properties influence important geological phenomena, including the development of abnormally high fluid pressures in sedimentary strata and migration of petroleum (Powers, 1967; Burst, 1969; Bruce, 1984). Thus, it is important to understand (a) how illite and smectite are interstratified and (b) the structural characteristics of poorly crystalline I/S prior to transformation to well-crystallized micas in high-temperature environments. However, there is considerable uncertainty about how illite and smectite are interstratified and even the extent to which they are intergrown. Some data from X-ray diffraction (XRD) and transmission electron microscopy (TEM) seem incompatible (Nadeau et al., 1984a, 1984b, 1984c; Ahn and Peacor, 1986a, 1986b). The present study was undertaken to reconcile these observations.

Most I/S shows Reichweite 0, 1, or 3 (R0, R1, and R3) ordering by XRD (Jagodzinski, 1949; Reynolds and Hower, 1970; Reynolds, 1980). It has been investigated in several TEM studies (e.g., Ahn and Peacor, 1986a; Klimentidis and Mackinnon, 1986; Yau et al., 1987; Hansen and Lindgreen, 1987; Huff et al., 1988; Veblen et al., 1990), and image simulations by Guthrie and Veblen (1989) showed that under special imaging conditions illite and smectite interlayers exhibit different contrast in TEM images.

Nadeau et al. (1984a, 1984b, 1984c) proposed that I/S that shows the XRD characteristics of R1 and R3 ordering consists mainly of 20- and 40-Å-thick "fundamental particles." They suggested that the interfaces between these particles are capable of absorbing water and organic molecules and thus behave like smectite interlayers, implying that materials yielding XRD patterns of I/S do not necessarily contain both illite and smectite interlayers. Nadeau et al. (1984b, 1984c, 1985) also suggested that individual fundamental particles are primary crystallization products rather than secondary particles disarticulated from larger crystals during sample preparation.

In contrast to the above, Ahn and Peacor (1986b) suggested that the smectite interlayers, being loosely bonded, are more easily cleaved than illite or mica-like interlayers; they concluded that thin flakes similar to the fundamental particles of Nadeau et al. (1984a, 1984b, 1984c) can be derived during sample preparation from larger crystals having two types of interlayers. Veblen et al. (1990) reported that illite- and smectite-layer ratios de-

0003–004X/90/0304–0267$02.00

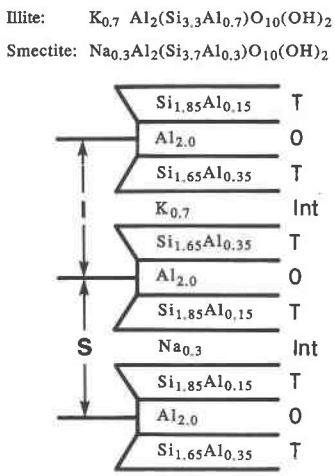

Fig. 1. Schematic diagram of ideal R1 I/S. The compositions of the tetrahedral (T) and octahedral (O) sheets and interlayers (Int) are indicated. The structure was assumed to be centered at the interlayers, resulting in two different tetrahedral sheets in a T-O-T layer (modified after Ahn and Peacor, 1986b).

termined from TEM images are consistent with those from XRD. Results of ^{29}Si NMR analyses also indicate that I/S contains both illite and smectite layers (Altaner et al., 1988), and Altaner et al. (1988) and Altaner and Bethke (1988) suggested that disarticulation at smectite interlayers may occur by osmotic swelling during the cation-saturation process. The high-resolution transmission electron microscopy (HRTEM) results reported here further support the idea that fundamental particles are, in fact, artifacts of sample preparation.

In the present study, chemically untreated R1 and R3 I/S were studied using HRTEM to investigate their layer stacking and the physical dimensions of crystals that apparently show the characteristics of fundamental particles. This study contains the first report of HRTEM images of I/S that show the details of stacking sequences. Such images provide data about the thicknesses of crystals that consist of structurally continuous 2:1 layers; thus, the physical dimensions of fundamental particles can be determined directly from the images. Image simulations were performed for I/S to identify theoretical differences between smectite and illite interlayers in HRTEM images and to determine the imaging conditions appropriate for interpretation of stacking arrangements.

Experimental

Three specimens that show typical R1 and R3 ordering by XRD were investigated. Sample MB 885 from the Mancos Shale (Nadeau and Reynolds, 1981; Keller et al., 1986) shows XRD patterns of R1 I/S with 30% expandable layers. The R3 I/S samples consist of (a) Kalkberg bentonite with 10% expandable layers from Cherry Valley, New York, and (b) a hydrothermal clay with 18% expandable layers from Zempleni, Hungary.

Ion-milled specimens were prepared from small chips following the method of Ahn and Peacor (1985). They were examined at 400 kV with a JEOL JEM 4000EX transmission electron microscope having a structure resolution limit of 1.7 Å and a spherical aberration coefficient (C_s) of 1.0 mm (Smith et al., 1986). A 40-μm objective aperture and a 150-μm condenser aperture were used for imaging.

The HRTEM imaging of I/S was difficult because the samples damage rapidly in the electron beam and because most crystals are bent and randomly oriented. The thin edges that are most appropriate for HRTEM imaging damage particularly rapidly in the electron beam. To reduce the effects of damage by the electron beam, specimens were examined at low beam intensity, and images were obtained at 150kX and 200kX, which are relatively low magnifications for HRTEM imaging. Proper defocus was achieved by changing focus slightly toward an underfocus condition from images having minimum contrast. Use of a TV monitor helped greatly.

TEM observations confirmed XRD data that the major sheet silicate in our samples is I/S; minor chlorite also occurs. Crystals showing the characteristics of detrital micas (Ahn and Peacor, 1986a) were not observed. The electron micrographs reported here are selected from among hundreds of images. Although we attempted to select representative images, the small sample sizes characteristic of HRTEM studies preclude certainty that HRTEM images are truly typical.

Image simulations

Simulated images of R1 I/S were obtained using Arizona State University multislice programs (O'Keefe et al., 1978; O'Keefe and Buseck, 1979). Image simulations were performed using the instrumental parameters given above, together with a beam divergence of 0.8 mrad and a defocus beam spread of 100 Å.

Smectite and illite are known to show a wide range of layer charges and compositions (Weaver and Pollard, 1973). In our image simulations, smectite was assumed to contain dehydrated interlayers, and smectite and illite layers were assumed to have the compositions $Na_{0.3}Al_2(Si_{3.7}Al_{0.3})O_{10}(OH)_2$ and $K_{0.7}Al_2(Si_{3.3}Al_{0.7})O_{10}(OH)_2$, respectively. Although such model compositions differ slightly from those of natural I/S, these approximate compositions can be used to determine how illite and smectite layers differ in TEM images.

Smectite and illite have 2:1 layer structures similar to micas (Hofmann et al., 1933; Grim et al., 1937), but structure refinements for I/S do not exist. Therefore, high-voltage electron-diffraction refinements of *1M* muscovite (Soboleva and Zvyagin, 1969) were used for both illite and smectite structures. An approximate R1 I/S structure with $C2/m$ symmetry was modeled based on the *1M* stacking of illite and smectite layers. Each layer was assumed to extend from octahedral to octahedral sheets (Fig. 1). Thus, interlayer positions fall within structural units rather than at their boundaries (Hower, 1967). Assuming that the illite and smectite layers extend from

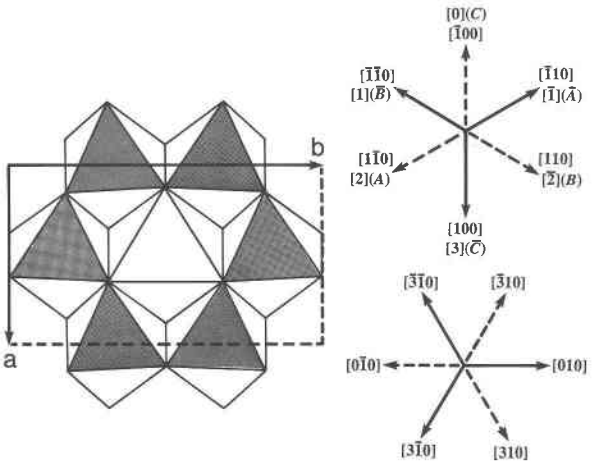

Fig. 2. The orientation relationship between zone axes and an octahedral sheet of *1M* mica (Soboleva and Zvyagin, 1969). Six zone axes that are related by $n(60)°$ rotations from the *a* axis are shown, with stacking symbols following those of Ross et al. (1966) and Zvyagin (1962).

one interlayer to another does not take into account the possible presence of two types of interlayers (Ahn and Peacor, 1986b).

Image-simulation results and interpretation

For the *1M* mica structure, "empty tunnels" in the interlayers can be viewed along six directions: [110], [100], [1Ī0], [Ī1̄0], [1̄00], and [Ī10]. These are related by $n(60)°$ rotations from the *a* axis and are shown in Figure 2 with the stacking symbols of Zvyagin (1962) and Ross et al. (1966). At high resolution the positions of such tunnels can be imaged under appropriate imaging condition as white spots and can be utilized for determining layer-stacking sequences (Iijima and Buseck, 1978; Amouric et al., 1981).

The images of ideal R1 mixed-layer I/S were simulated for six orientations. The results (Figs. 3a, 3b, 3c) show that circular white spots with an ~4.5-Å periodicity occur at a defocus (Δf) of −200 Å and appear in the positions of the tunnels at both illite and smectite interlayers. The spots become less prominent with decreasing Δf, and they appear rectangular and less well defined at Scherzer focus (−490 Å).

In simulated images at $\Delta f = -200$ Å, the white spots at smectite interlayers are more diffuse than those at illite interlayers; the tunnels are also less well defined when fewer alkali cations are present. Ideally, the differences in these spots could be used for distinguishing smectite from illite interlayers in HRTEM images. However, the exact positions of the spots in alkali-deficient 2:1 layer silicates may be more difficult to determine because the spots are more diffuse. The simulations for 125-kV TEM images of Guthrie and Veblen (1989) also showed that the shapes and sizes of white spots of illite and smectite interlayers differ.

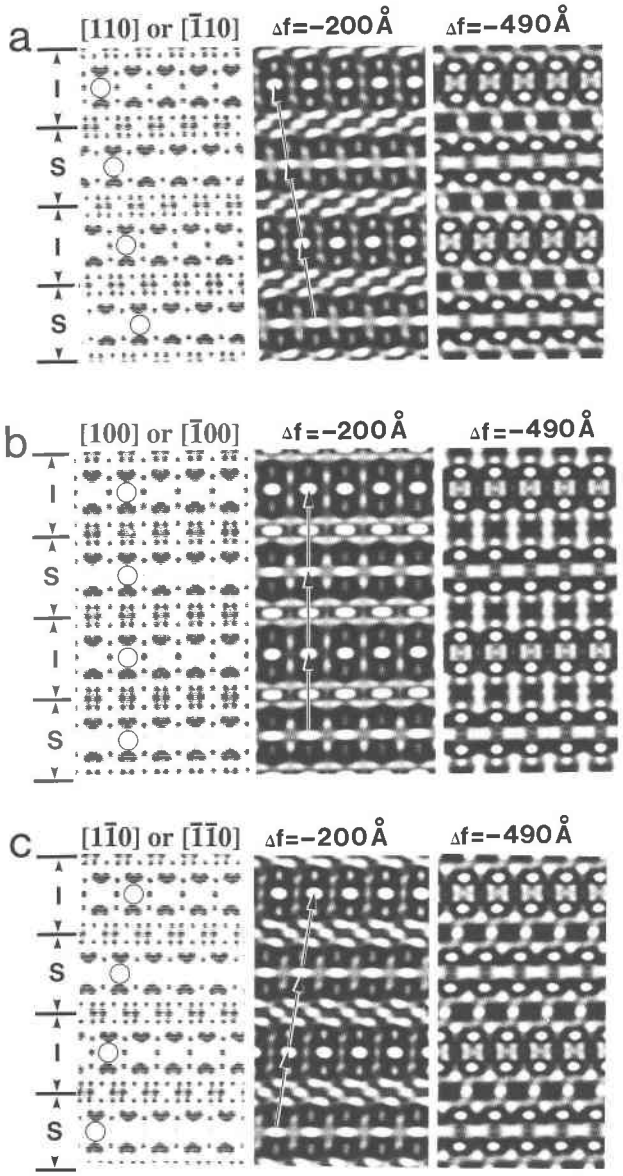

Fig. 3. Projected crystal potentials (left sides) and simulated images (center and right sides of figures) of ideal R1 I/S as viewed down the (a) [110] or [1̄10], (b) [100] or [1̄00], and (c) [1Ī0] or [Ī1̄0] directions of Δf values of −200 and −490 Å. I and S denote illite and smectite layers, respectively. The open circles mark the positions of "empty tunnels," as discussed in the text, and the PSVs are drawn onto the calculated images. The objective aperture (radius = 0.6 Å^{-1}) is centered on the incident beam, and a crystal thickness of 150 Å and accelerating voltage of 400 kV are used.

The relative stacking orientations of individual layers can be visualized by drawing lines from a white spot in one interlayer region to the closest white spots of adjacent layers (Iijima and Buseck, 1978). Such connecting lines represent projected stacking vectors (PSVs). For [110] (or [1̄10]) images (Fig. 3a), the angle between the PSV and (001) is approximately 99.73° (when $\beta = 101.20°$, which

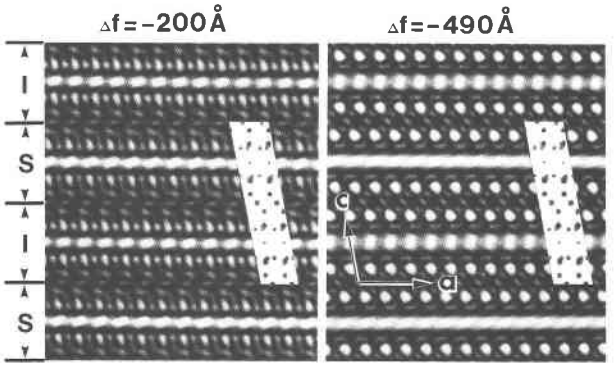

Fig. 4. Simulated [010] images of ideal R1 I/S at −200 and −490 Å defocus. The insets represent the crystal potential of one unit cell. Simulations were performed using the same instrumental and electron-optical parameters as for Fig. 4.

is the case for the *1M* muscovite refined by Soboleva and Zvyagin, 1969). Images for [100] (or [$\bar{1}$00]) (Fig. 3b) result in PSVs that are perpendicular to the (001) basal planes. Simulated images obtained along [1$\bar{1}$0] (or [$\bar{1}\bar{1}$0]) (Fig. 3c) show PSVs that are tilted at the same angle as [110] (or [$\bar{1}$10]) images but in the opposite directions.

Only three distinct angles exist between PSVs and (001) planes, and so [110], [100], and [1$\bar{1}$0] images cannot be distinguished from [$\bar{1}$10], [$\bar{1}$00], and [$\bar{1}\bar{1}$0] images, respectively, in the *1M* mica structure. Except for some Li-micas, the stacking rotations of most micas are $n(120)°$ (Radoslovich, 1959; Ross et al., 1966). In this study, the stacking rotations of I/S were assumed to be restricted to $n(120)°$, so the relative orientations of stacked layers can be interpreted from a single orientation.

Other tunnels at interlayers of micas can be projected for [010], [310], [3$\bar{1}$0], [0$\bar{1}$0], [$\bar{3}\bar{1}$0], and [$\bar{3}$10] orientations, which are related by $n(60)°$ rotations from the *b* axis (Fig. 2). Image simulations for these orientations show that tunnels with a 2.6-Å periodicity can be imaged using the JEOL JEM 4000EX electron microscope (Fig. 4). However, their projected sizes are smaller, and the white spots have shorter periodicities than those for the previous six orientations. The diffuseness of the spots of smectite interlayers is also evident for these orientations. The image at Scherzer focus (Fig. 4) shows two rows of large white spots that correspond to tunnels between cations in the tetrahedral and octahedral sheets in a 2:1 layer. Similar spots were imaged for minnesotaite and utilized for determining the widths of tetrahedral strips (Ahn and Bu-

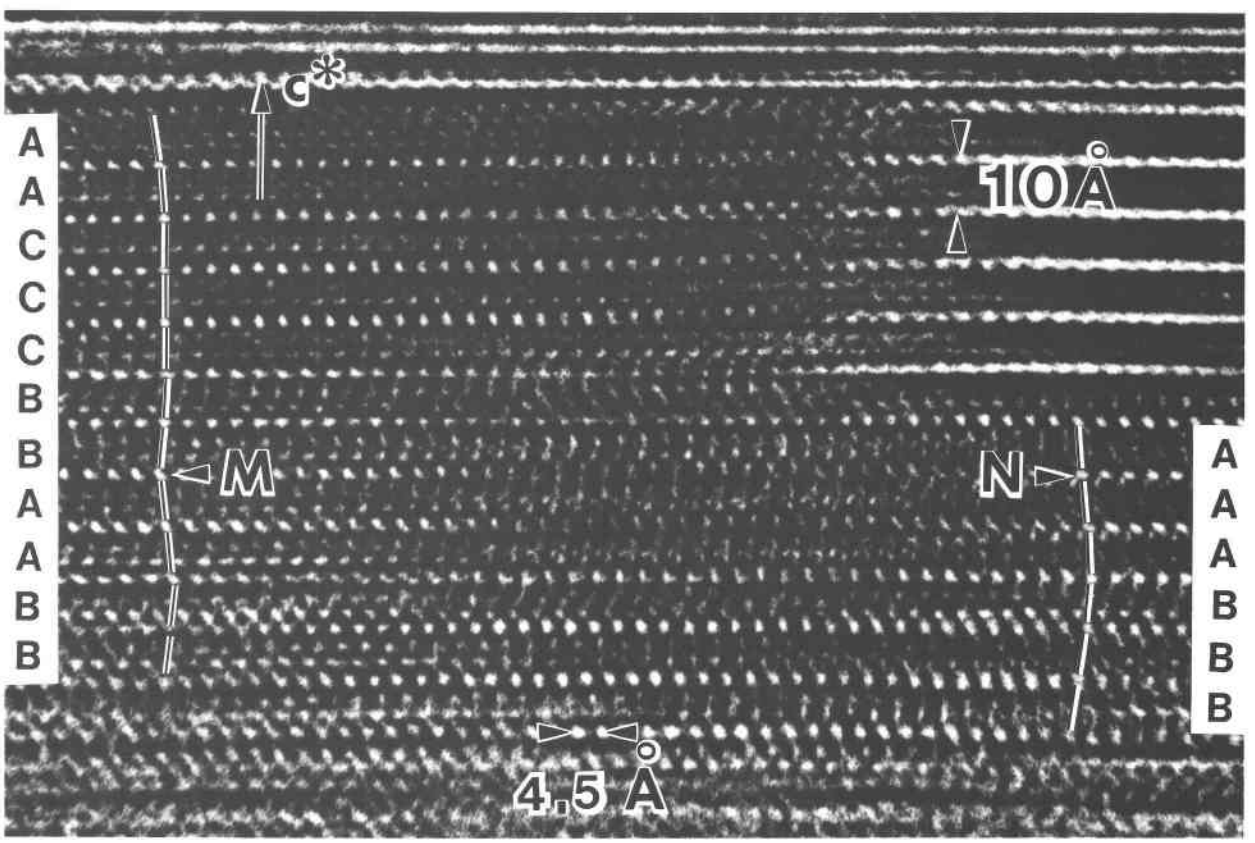

Fig. 5. Structure image of sample MB 885 showing white spots with 4.5-Å periodicities. PSVs and Zvyagin symbols are marked on the image. Although a stacking fault occurs at M, none is present at N. The white spots between M and N are indistinct as a result of structural distortions.

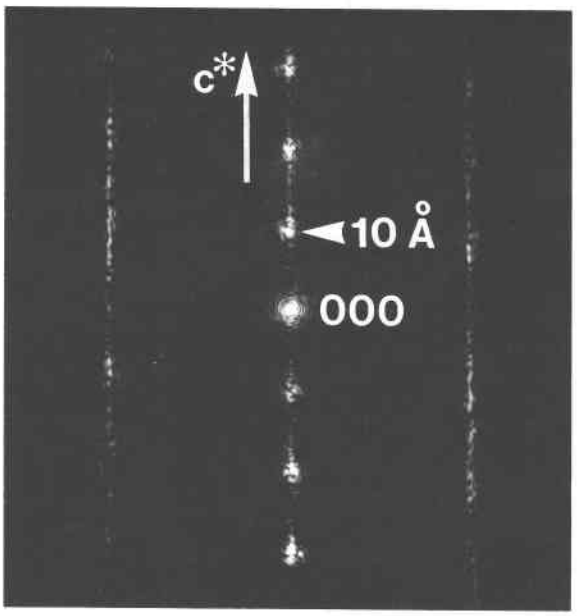

Fig. 6. Optical diffraction pattern from the image of Fig. 5. The central row contains distinct 00*l* reflection spots at 10-Å spacings (arrow), whereas spots in both adjacent rows are dispersed parallel to c* (see text).

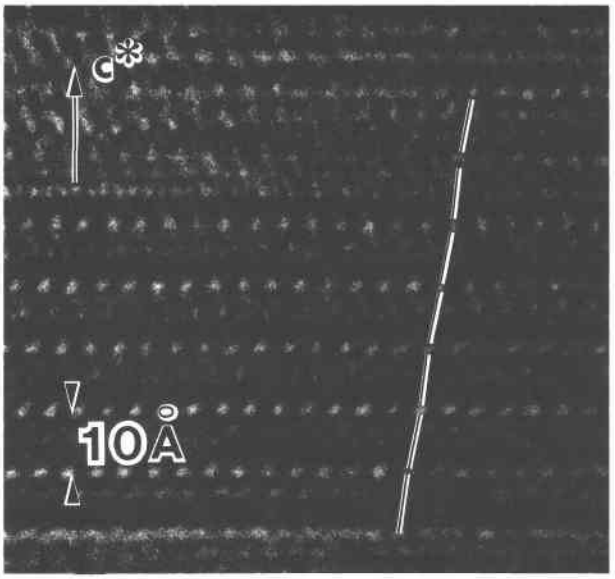

Fig. 8. Structure image from the Zempleni sample. The layers show *1M* stacking, and no stacking faults occur. The angles between PSVs and (001) of individual layers vary slightly.

seck, 1989). However, the white spots at the interlayers of I/S in these projections are difficult to use for determining the relative stacking rotations because they display no significant differences in the angles between PSVs and (001).

Experimental HRTEM images

For all three samples examined here, distinct white spots with a 4.5-Å periodicity at the interlayers appear at a slight underfocus ($\Delta f \simeq -200$ Å), in agreement with the image simulations. Such interpretable two-dimensional images that contain information about the positions of small groups of atoms will be called "structure images" in this discussion (e.g., Buseck and Iijima, 1974; Iijima and Buseck, 1978), although ideal structure images are only obtained at rather special experimental conditions (Spence, 1988). The stacking orientations of individual layers in some images are marked using Zvyagin symbols (cf. Iijima and Buseck, 1978); PSVs have been drawn onto the images.

A structure image of specimen MB 885 (R1) shows highly disordered stacking (Fig. 5). The observed se-

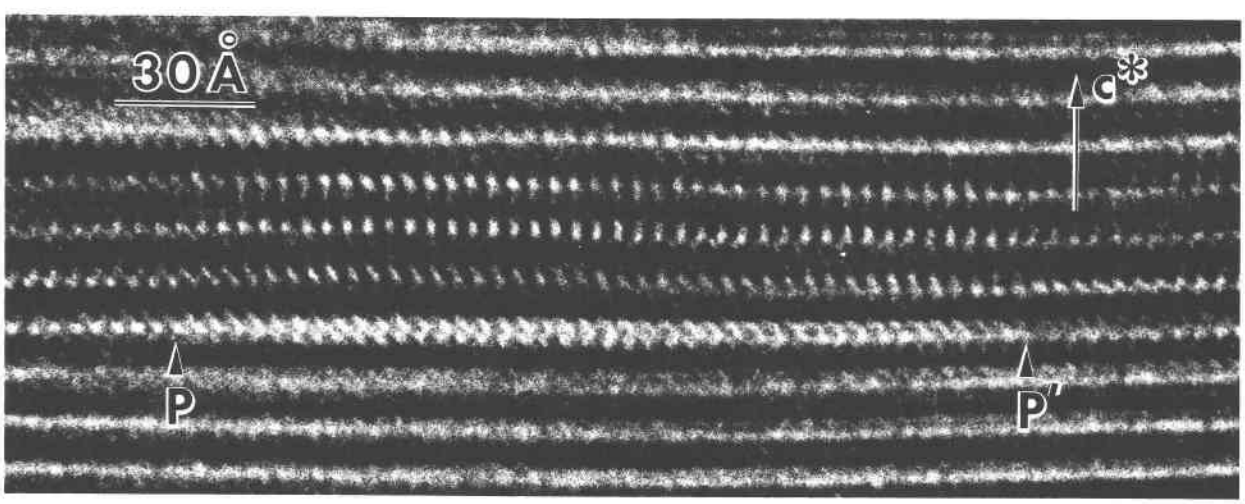

Fig. 7. Structure image of sample MB 885 showing relatively few layers that are related by white spots. A wider white fringe, which apparently corresponds to a slightly separated interlayer region, occurs between P and P'.

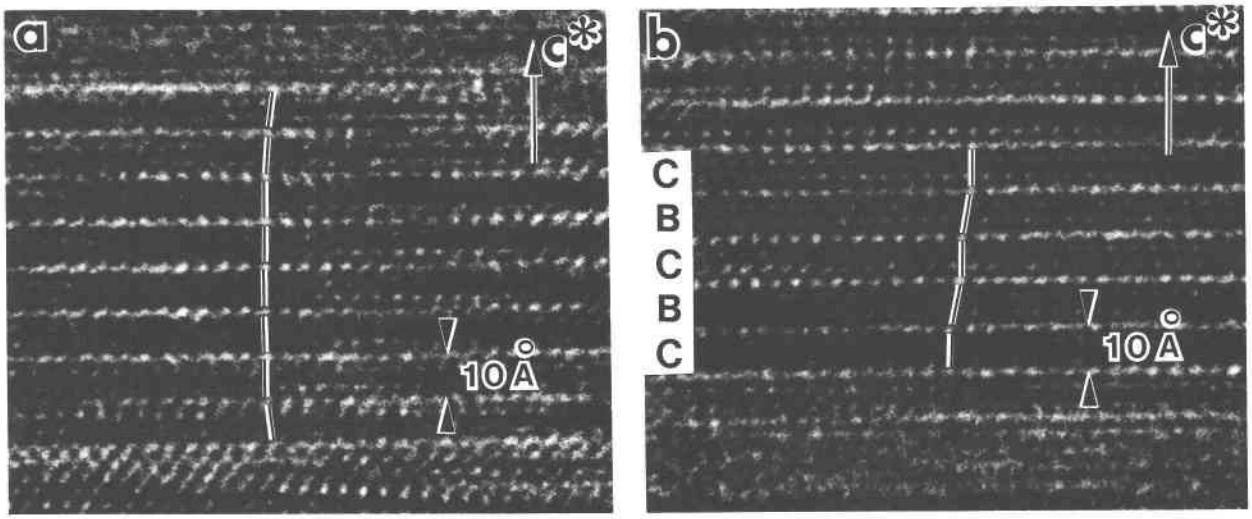

Fig. 9. Structure images from the Kalkberg sample. (a) The T-O-T layers are stacked regularly in the central portion of the crystal, but the stacking changes at the top and bottom of the image. (b) Part of the crystal shows two-layer stacking. Zvyagin symbols are marked.

quence (BBAABBCCCAA) indicates that stacking faults limit units showing apparent *1M* stacking to two or three layers. When the white spots at the interlayers are traced from layer to layer, the angles between PSVs and (001) change slightly, even though the PSVs are slanted in the same direction. An optical diffraction pattern (Fig. 6) of the area of Figure 5 contains $1\bar{1}l$, $11l$, and $02l$ reflections that are scattered in the rows parallel to **c*** on both sides of the $00l$ reflection row. These reflections indicate that individual unit layers have slightly different β values.

Although most structure images of R1 I/S show eight- to ten-layer units that can be connected by PSVs, relatively thin packets of layers showing white spots also occur (Fig. 7). The image shows at least four successive interlayers with white spots, indicating that at least five 2:1 layers are stacked coherently.

Structure images of R3 I/S samples also contain extensive areas that can be connected by PSVs. The image in Figure 8 is of an R3 sample (Zempleni) projected along the $[1\bar{1}0]$ (or $[\bar{1}\bar{1}0]$) zone axis. The PSVs are tilted in the same direction, indicating that the marked area shows *1M* stacking. Such regions that are free of stacking faults over eight or more layers are uncommon in I/S samples. The angles between the PSVs and (001) differ slightly, indicating slight variations in the β values of individual layers.

In Figure 9a, the layers at the center of the image have [0](C) or [3]($\bar{\text{C}}$) orientations. However, the stackings differ at the top and bottom of the image, and at the figure edges the white spots are indistinct. Figure 9b shows an image in which two repeats of two-layer stacking can be identified. If the stacking rotation is restricted to $n(120)°$, the stacking sequence is $[\bar{2}0\bar{2}0]$(BCBC), which is a $2M_1$ sequence.

Most I/S crystals are slightly curved. Parts of the crystals are therefore commonly slightly out of the Bragg-diffraction condition, and the white spots along a series of end-to-end PSVs do not display equal intensities and sharpness. Therefore, accurate positions of the spots are difficult to determine. Portions of most crystals that can be connected with white spots at the interlayers are thicker than seven or eight layers, and the packets that have coherent stacking may actually be thicker than those shown in the structure images.

Discussion

Structural disorder in I/S

The minor variations in β values of some layers, as indicated by the observed angles between the PSVs and (001) of individual layers, presumably occur because of slight structural differences between illite and smectite, minor structural distortions, or both. As a result of the similar interlayer spacings of illite and collapsed smectite, the layers cannot be distinguished unambiguously in TEM images. The differences in appearance of the white spots in simulated images (Fig. 3) are not evident in the experimental images.

The $1M_d$ stacking sequence is thought to be dominant in I/S (Hower and Mowatt, 1966; Środoń and Eberl, 1984), although some XRD studies suggest the occurrence of *1M* and $2M_1$ polymorphs in illite-rich I/S (Inoue et al., 1987; Austin et al., 1989). Structure images show that *1M* stacking in I/S is interrupted by stacking faults, and apparent *1M* stacking occurs for only a few 2:1 layers in most crystals. It seems plausible that the $1M_d$ stacking proposed by Yoder and Eugster (1954, 1955) results from narrow regions of *1M* material that are offset by randomly spaced stacking faults, as is shown in our images. However, slightly different β angles in stacked 2:1 layers sug-

gest that minor structural heterogeneities may also contribute to the features seen by XRD. These layer-to-layer differences reduce the phase coherence of X-ray scattering between the stacked layers, and reflection spots other than 00*l* are diffuse.

Drits (1987) showed that XRD patterns are not sufficiently sensitive to reveal the degree of heterogeneity in I/S, and he suggested that "precise studies are therefore required to reveal the existence of homogeneous, quasi-homogeneous, and heterogeneous mixed-layer samples." Individual smectite and illite layers can have a broad range of composition, and existing analyses presumably represent only the average compositions of heterogeneous I/S (Ahn and Peacor, 1986a). Many XRD studies indicate that $1M_d$ sheet silicates decrease in abundance with increasing metamorphic grade (Reynolds, 1963; Hower and Mowatt, 1966; Maxwell and Hower, 1967); the structural disorder and probable chemical heterogeneity inferred from the HRTEM data presumably decrease and eventually disappear during the transition to more stable $1M$ or $2M_1$ illite (or muscovite) with increasing temperature. Both structural heterogeneity and stacking disorder are apparently characteristic of $1M_d$ I/S, and some of the features in structure images may be related to the chemical heterogeneity of individual layers.

Implications of HRTEM data for fundamental particles

Nadeau et al. (1984c) defined fundamental particles as "individual or fine particles that yield a single-crystal pattern by electron diffraction." They also stated that fundamental particles are individual crystals rather than crystal fragments. The available data about the thicknesses of fundamental particles are based on measurement of replicas of Pt-shadowed flakes, some of which might be disarticulated particles produced during sample preparation.

TEM investigations of ion-milled specimens showed large regions containing lattice fringes with periodicities that were suggested as representing mixed layering of illite and smectite (Hansen and Lindgreen, 1987; Ahn and Peacor, 1989; Jiang et al., 1989; Veblen et al., 1990). In addition, mixed layering was demonstrated in TEM studies of rectorites (McKee and Buseck, 1978; Klimentidis and Mackinnon, 1986; Ahn and Peacor, 1986b). However, lattice-fringe images do not contain information regarding structural coherency between stacked 2:1 layers, and Nadeau (1986) suggested that areas of lattice fringes that are thicker than fundamental particles consist of aggregates of fundamental particles having a high degree of face-to-face orientation.

Using HRTEM, the interlayers between structurally continuous 2:1 layers can be distinguished from those between layers having simple face-to-face contact but no structural continuity. In single crystals of micas, the 2:1 layers maintain coherent stackings related by $n(120)°$ or $n(60)°$ rotations, and HRTEM images at appropriate orientations show periodic white spots (Fig. 3). However, there is no necessary structural continuity between stacked aggregates. Their interfaces can occur without any specific layer-to-layer crystallographic relationships and so would not be expected to show periodic white spots in structure images.

If the I/S showing R1 or R3 ordering in XRD patterns consisted of fundamental particles, the thicknesses of packets that show continuous rows of white spots should be dominated by two- and four-layer units, respectively. However, our HRTEM observations of both R1 and R3 samples indicate that packets having coherent stacking arrangements are thicker than the predicted two or four layers and thus are inconsistent with the hypothesis of fundamental particles.

Such disagreement can be resolved if weakly bonded smectite interlayers disarticulate more easily than illite interlayers (Ahn and Peacor, 1986b). Crystal-thickness measurements of Pt-shadowed particles by Nadeau and coworkers are based on <0.1- or <0.2-μm fractions. It is thus possible that disarticulated particles are concentrated during the laboratory separation process. However, the specimens investigated in the present study were prepared by ion-milling of petrographic thin sections, which avoids the creation of disarticulated thin particles. The fundamental particles of Nadeau and coworkers are apparently secondary crystallites that were originally parts of larger crystals that contained two types of interlayers.

$2M_1$ stacking sequences in I/S

During burial or contact metamorphism, $1M_d$ I/S reacts to form $1M$ illite (or muscovite), which then transforms to $2M_1$ muscovite at higher temperatures (Velde and Hower, 1963; Maxwell and Hower, 1967; Hoffman and Hower, 1979; Lee et al., 1985). Our HRTEM images indicate that most layer stackings in the I/S samples we studied are consistent with $1M_d$ sequences. Areas having $1M$ stacking occur, but they are uncommon. Although two units of $2M_1$-type stacking were observed in an R3 I/S sample, extensive $2M_1$ stacking sequences were not identified. Short repeats of $2M_1$ occur in I/S, apparently because, by analogy to the pyriboles (Veblen and Buseck, 1979), disordered stacking sequences can result in the appearance of locally ordered stacking.

Lattice fringes of areas with $2M_1$ stacking would show 2-layer periodicities that resemble those of areas having R1 mixed layering, as demonstrated in the simulations of Guthrie and Veblen (1989). If $2M_1$ stacking actually occurs in I/S, as indicated in XRD studies (Inoue et al., 1987; Austin et al., 1989), care will be required to correctly interpret two-layer periodicities in lattice-fringe images of I/S. However, in the specimens we studied, $2M_1$ stacking is rare, and so we conclude that most two-layer periodicities of I/S lattice fringes represent mixed layering.

Conclusions

1. The stacking of individual 2:1 layers of I/S can be interpreted in the same way as micas (Iijima and Buseck,

1978; Amouric et al., 1981). In JEOL JEM 4000EX TEM images, at $\Delta f \simeq -200$ Å the positions of the white spots in the two types of interlayers correspond to the "empty tunnels."

2. Image simulations imply that illite and smectite interlayers can ideally be distinguished in structure images, but they could not be unambiguously differentiated in our experimental HRTEM images.

3. Most R1 and R3 I/S crystals show $1M_d$ stacking sequences in which $1M$ stacking is interrupted by abundant stacking faults.

4. Structure images show that individual layers within I/S have slightly different β angles, suggesting that such structural heterogeneity as well as stacking disorder may account for the characteristic weakness or absence of *hkl* reflections in XRD patterns of $1M_d$ materials.

5. Localized $2M_1$-type sequences in R3 I/S may result from random stacking in disordered material.

6. Most regions of crystals showing coherent stacking relationships are thicker than the hypothesized fundamental particles of Nadeau and coworkers. Thus, our HRTEM data suggest that these "fundamental particles" are artifacts of sample preparation and not primary crystallites.

Acknowledgments

We are grateful to R. C. Reynolds for discussion and providing samples and XRD data. The hydrothermal clay from Zempleni, Hungary, was collected by Jan Środoń. We thank A. Inoue, I. Mackinnon, and R. J. Kirkpatrick for reviews, and many suggestions were also provided by D. R. Peacor and D. R. Veblen. We thank Sue Selkirk for drafting. Electron microscopy and image simulation were performed at the Facility for High Resolution Electron Microscopy at Arizona State University, supported by NSF and ASU. This study was supported by NSF grant EAR870529.

References cited

Ahn, J.H., and Buseck, P.R. (1989) Microstructures and strip-width order and disorder in Fe-rich minnesotaites. American Mineralogist, 74, 384–393.

Ahn, J.H., and Peacor, D.R. (1985) Transmission electron microscopic study of diagenetic chlorite in Gulf Coast argillaceous sediments. Clays and Clay Minerals, 33, 228–236.

——— (1986a) Transmission and analytical electron microscopy of the smectite-to-illite transition. Clays and Clay Minerals, 34, 165–179.

——— (1986b) Transmission electron microscope data for rectorite: Implications for the origin and structure of "fundamental particles." Clays and Clay Minerals, 34, 180–186.

——— (1989) Illite/smectite from Gulf Coast shales: A reappraisal of transmission electron microscope images. Clays and Clay Minerals, 37, 542–546.

Altaner, S.P., and Bethke, C.M. (1988) Interlayer order in illite/smectite. American Mineralogist, 73, 766–774.

Altaner, S.P., Weiss, C.A., Jr., and Kirkpatrick, R.J. (1988) Evidence from ^{29}Si NMR for the structure of mixed-layer illite/smectite clay minerals. Nature, 331, 699–702.

Amouric, M., Mercuriot, G., and Baronnet, A. (1981) On computed and observed HRTEM images of perfect mica polytypes. Bulletin de Minéralogie, 104, 298–313.

Austin, G.S., Glass, H.D., and Hughes, R.E. (1989) Resolution of the polytype structures of some illitic clay minerals that appear to be $1M_d$. Clays and Clay Minerals, 37, 128–134.

Bruce, C.H. (1984) Smectite dehydration—Its relation to structural development and hydrocarbon accumulation in northern Gulf of Mexico Basin. American Association of Petroleum Geologists Bulletin, 68, 673–683.

Burst, J.R. (1969) Diagenesis of Gulf Coast clayey sediments and its possible relation to petroleum migration. American Association of Petroleum Geologists Bulletin, 53, 73–93.

Buseck, P.R., and Iijima, S. (1974) High resolution electron microscopy of silicates. American Mineralogist, 59, 1–21.

Drits, V.A. (1987) Mixed-layer minerals: Diffraction methods and structural features. In L.G. Schultz, H. van Olphen, and F.A. Mumpton, Eds., Proceedings of the International Clay Conference, Denver, 1985, p. 33–45. Clay Minerals Society, Bloomington, Indiana.

Grim, R.E., Bray, R.M., and Bradley, W.F. (1937) The mica in argillaceous sediments. American Mineralogist, 22, 813–829.

Guthrie, D.G., and Veblen, D.R. (1989) High resolution transmission electron microscopy of mixed-layer illite/smectite: Computer simulations. Clays and Clay Minerals, 37, 1–11.

Hansen, P.L., and Lindgreen, H. (1987) Structural investigations of mixed-layer smectite-illite clay minerals from North Sea oil rocks. In G.W. Bailey, Ed., Proceedings of 45th Annual Meeting of Electron Microscope Society of America, p. 374–375. San Francisco Press, San Francisco.

Hoffman, J., and Hower, J. (1979) Clay mineral assemblages as low grade metamorphic geothermometers: Application to the thrust faulted Disturbed Belt of Montana, U.S.A. Society of Economic Paleontologists and Mineralogists Special Publications, 26, 55–79.

Hofmann, U., Endell, K., and Wilm, D. (1933) Kristallstruktur und Quellung von Montmorillonit. Zeitschrift für Kristallographie, 86, 340–348.

Hower, J. (1967) Order of mixed-layering in illite/montmorillonite. In S.W. Bailey, Ed., Clays and clay minerals, Proceedings of 15th National Conference, Pittsburgh, Pennsylvania, 1966, p. 63–74. Pergamon Press, New York.

Hower, J., and Mowatt, T.C. (1966) The mineralogy of illite and mixed-layer illite/montmorillonites. American Mineralogist, 51, 825–854.

Huff, W.D., Whiteman, J.A., and Curtis, C.D. (1988) Investigation of a K-bentonite by X-ray powder diffraction and analytical transmission electron microscopy. Clays and Clay Minerals, 36, 83–93.

Iijima, S., and Buseck, P.R. (1978) Experimental study of disordered mica structures by high-resolution electron microscopy. Acta Crystallographica, A34, 709–719.

Inoue, A., Kohyama, N., Kitangawa, R., and Watanabe, T. (1987) Chemical and morphological evidence for the conversion of smectite to illite. Clays and Clay Minerals, 35, 111–120.

Jagodzinski, H. (1949) Eindimensionale Fehlordnung in Kristallen und ihr Einfluß auf die Röntgeninterferenzen. I. Berechnung des Fehlordnungsgrades aus der Röntgenintensitäten. Acta Crystallographica, 2, 201–207.

Jiang, W.-T., Peacor, D.R., Merriman, R.J., and Roberts, B. (1989) STEM study of ordered mixed-layer illite/smectite formed as an alteration product of illite. EOS, 70, 353.

Keller, W.D., Reynolds, R.C., and Inoue, A. (1986) Morphology of clay minerals in the smectite-to-illite conversion series by scanning transmission electron microscopy. Clays and Clay Minerals, 34, 187–197.

Klimentidis, R.E., and Mackinnon, I.D.R. (1986) High-resolution electron microscopy of ordered mixed-layer clays. Clays and Clay Minerals, 34, 155–164.

Lee, J.H., Peacor, D.R., Lewis, D.D., and Wintsch, R.P. (1985) Chlorite-illite/muscovite interlayered and interstratified crystals: A TEM/STEM study. Contributions to Mineralogy and Petrology, 88, 372–385.

Maxwell, D.T., and Hower, J. (1967) High-grade diagenesis and low-grade metamorphism of illite in the Precambrian Belt series. American Mineralogist, 52, 843–857.

McKee, T.R., and Buseck, P.R. (1978) HRTEM observation of stacking and ordered interstratification in rectorite. In J.M. Sturgess, Ed., Electron microscopy 1978, vol. 1, p. 272–273. Microscopical Society of Canada, Toronto, Canada.

Nadeau, P.H. (1986) The physical dimensions of fundamental clay particles. Clay Minerals, 20, 499–514.

Nadeau, P.H., and Reynolds, R.C., Jr. (1981) Burial and contact metamorphism in the Mancos Shale. Clays and Clay Minerals, 29, 249–259.

Nadeau, P.H., Tait, J.M., McHardy, W.J., and Wilson, M.J. (1984a) In-

terstratified XRD characteristics of physical mixtures of elementary clay particles. Clay Minerals, 19, 67–76.

Nadeau, P.H., Wilson, M.J., McHardy, W.J., and Tait, J.M. (1984b) Interstratified clays as fundamental particles. Science, 225, 923–925.

——— (1984c) Interparticle diffraction: A new concept for interstratified clays. Clay Minerals, 19, 759–769.

——— (1985) The conversion of smectite to illite during diagenesis: Evidence from some illitic clays from bentonite and sandstones. Mineralogical Magazine, 49, 393–400.

O'Keefe, M.A., and Buseck, P.R. (1979) Computation of high resolution TEM images of minerals. American Crystallographic Association Transactions, 15, 27–44.

O'Keefe, M.A., Buseck, P.R., and Iijima, S. (1978) Computed crystal structure images for high resolution electron microscopy. Nature, 274, 322–324.

Powers, M.C. (1967) Fluid-release mechanisms in comparing marine mudrocks and their importance in oil exploration. American Association of Petroleum Geologists Bulletin, 51, 1240–1254.

Radoslovich, E.W. (1959) Structural control of polymorphism in micas. Nature, 183, 253.

Reynolds, R.C., Jr. (1963) Potassium-rubidium ratios and polymorphism in illite and microclines from the clay size fraction of Proterozoic carbonate rocks. Geochimica et Cosmochimica Acta, 27, 1097–1112.

——— (1980) Interstratified clay minerals. In G.W. Brindley and G. Brown, Eds., Crystal structures of clay minerals and their X-ray identification, p. 249–303. Mineralogical Society, London.

Reynolds, R.C., Jr., and Hower, J. (1970) The nature of interlayering in mixed-layer illite/montmorillonite. Clays and Clay Minerals, 18, 25–36.

Ross, M., Takeda, H., and Wones, D.R. (1966) Mica polytypes: Systematic description and identification. Science, 151, 191–193.

Smith, D.J., Barry, J.C., Bursill, L.A., Petford, A.K., and Wheatley, J.C. (1986) Atomic resolution imaging of crystalline defects and surfaces. JEOL News, 24E, 2–6.

Soboleva, S.V., and Zvyagin, B.B. (1969) Crystal structure of dioctahedral Al-mica *1M*. Soviet Physics–Crystallography, 13, 516–520.

Spence, J.C.H. (1988) Experimental high-resolution electron microscopy (2nd edition), 427 p. Clarendon Press, Oxford.

Środoń, J., and Eberl, D.D. (1984) Illite. In Mineralogical Society of America Reviews in Mineralogy, 13, 495–544.

Veblen, D.R., and Buseck, P.R. (1979) Chain-width order and disorder in biopyriboles. American Mineralogist, 64, 687–700.

Veblen, D.R., Guthrie, G.D., Livi, K.J.T., and Reynolds, R.C. (1990) High-resolution transmission electron microscopy and electron diffraction of mixed-layer illite/smectite: Experimental results. Clays and Clay Minerals, 38, 1–13.

Velde, B., and Hower, J. (1963) Petrological significance of illite polymorphism in Paleocene sedimentary rocks. American Mineralogist, 48, 1239–1254.

Weaver, C.E., and Pollard, L.D. (1973) The chemistry of clay minerals, 213 p. Elsevier, Amsterdam.

Yau, Y.C., Peacor, D.R., and McDowell, S.D. (1987) Smectite-illite reaction in Salton Sea shales. Journal of Sedimentary Petrology, 57, 335–342.

Yoder, H.S., and Eugster, H.P. (1954) Phlogopite synthesis and stability range. Geochimica et Cosmochimica Acta, 6, 157–185.

——— (1955) Synthetic and natural muscovites. Geochimica et Cosmochimica Acta, 8, 225–280.

Zvyagin, B.B. (1962) A theory of polymorphism of micas. Soviet Physics–Crystallography, 6, 571–580.

MANUSCRIPT RECEIVED JANUARY 26, 1989
MANUSCRIPT ACCEPTED NOVEMBER 20, 1989